JMEPEG (2001) 10:419–428

Improvement of the Liquid Segregation Phenomena of Semisolid Aluminum Alloys by the Multistage Strain Rate Control in the Compression Test

C.G.Kang and K.D. Jung

(Submitted 17 July 2000; in revised form 17 January 2001)

The deformation behavior of semisolid aluminum alloys in the range of solid fraction (f_s) between 55 and 90% was investigated through compression tests for the variation of strain rate. In order to obtain the optimal conditions of the net shape forging process, the rheological behavior of aluminum alloy in the semisolid state has been examined by using parallel plate compression. The strain rate is the value of the strain rate corresponding to the stress to avoid the liquid segregation phenomena during compression tests. The material constants of semisolid material in the stress-strain curve are proposed to perform the numerical analysis for a die design of semisolid forging. The starting materials used in this experiment are A357, 86S (similar to A319), and A390 alloys, which are fabricated by the electromagnetic stirring process. The intelligent compression test with a controlled strain rate was performed. The liquid segregation in the overall cross-sectional areas is controlled as the multistage variation of the pressing velocity and variation of the solid fraction during the compression process. The characteristics of materials flow between solid and liquid phases, considering the liquid segregation, are discussed for various solid fractions and pressing velocities.

Keywords liquid segregation, multistage variation of pressing velocity, semisolid forging, semisolid material, solid fraction

1. Introduction

Semisolid forming is performed in the coexisting solidus-liquidus phase. The characteristics of semisolid forming can decrease defects such as segregation and porosity because of the improvement in fluidity in a globular microstructure state. This way of forming difficult-to-machine materials is very helpful because there is much less deformation resistance compared with conventional forging processes. In addition, productivity can be improved because of the formation at smaller loads. Thus, the semisolid forming process is now becoming increasingly popular for the manufacturing of the net shape parts and has been spread and studied around the world.[1–5]

In a study of the deformation behavior of semisolid materials (SSMs), Suery and Flemings[6] studied the deformation behavior of an Sn-15% Pb alloy in the semisolid state. Yosida *et al.*[7] observed the microstructure and the flow phenomenon with an Al-4.5% Cu alloy in the semisolid forging process. Gunasekera[8] published the constitutive equation of SSMs using the geometric shape of a solid particle and of a liquid. Pinsky *et al.*[9] proposed that liquid segregation increases as the friction between the die and the material becomes higher. Kiuchi *et al.*[10] investigated the deformation resistance of semisolid metals. Most of the published reports that have been performed are about the properties of SSM and the effects of strain rate on the macroscopic behavior in the compression forming of semisolid aluminum alloys. The most important problem regarding the semisolid forming process is the prevention of the liquid segregation phenomena during deformation. Since the liquid is of eutectic composition in materials, the liquid segregation will result in a significant or undesirable situation.

In this work, thus, the compression experiments were carried out to investigate the deformation behavior of SSMs for the variation of main process variables such as the compression velocity and the solid fraction (f_s). The relationship between the strain rate and the stress was also suggested to control the liquid segregation phenomenon. By using the proposed relationship, this validity was experimentally proved. These proposed stress-strain curves and material parameters would be applied to the die design in the development of components in the future.

C.G. Kang, School of Mechanical Engineering, Engineering Research Center for Net Shape and Die Manufacturing (ERC/NSDM), Pusan National University. **K.D. Jung,** Graduate School, Department of Mechanical and Precision Engineering, Pusan National University, Pusan 609-735, Korea. Contact e-mail: cgkang@hyowon.pusan.ac.kr.

2. The Experiments

2.1 Compression Experiments

The starting materials used in this study were A357, 86S (similar to A319), and A390 materials fabricated by the electromagnetic stirring process and made by Pechiney (Voreppe, France). The chemical compositions of these materials are shown in Table 1.

For the compression forming in the semisolid state, the reheating time at the elevated temperature that corresponds to the solid fraction is important. Therefore, in this study, the compression experiments were carried out after heating for 10 min at the temperatures corresponding to the solid fractions of 55, 70, and 90%.

After machining the compression specimen ψ (diameter) $\times$

h (height) = 17 × 17mm, the compression test on the SSM was performed by using an apparatus of the Material Testing System (MTS), attaching an electric furnace to increase the temperature up to that of the desired solid fraction. The liquid segregation in the overall cross-sectional areas was controlled as the multistage variation of the strain rate during the compression process. Figure 1 shows an MTS machine with a maximum load of 25 tons used for the compression of the semisolid aluminum alloy.

2.2 The Results of Compression Experiments

Figure 2(a) and (b) show the curves of true stress-true strain according to the change of die velocities (V_{die} = 1, 10, 100, 500, and 1000 mm/s) at the temperatures of ① and ② and in Table 2. The strain rate is defined as $\dot{\varepsilon} = V_{die}/h$ (h is the specimen height, and V_{die} is the compression velocity). For the deformation characteristics of SSMs, the stress increases up to a specific strain value (0.1 in Fig. 2a and b). However, from the strain of $\varepsilon = 0.1$, the stress decreases remarkably when the strain rate increases. This phenomenon is explained by liquid flow being activated and transferred to the free surface at the specific strain rate, even though the stress increases for densification of the structure and stimulation of liquid flow from the first moment. Because of liquid segregation, the load is decreased by cracking on the surface of the specimen and the separation of the solid-liquid region; it is then increased by plastic deformation of the solid region after the structure of the materials experiences some densification.[11,12] In the compression forming of an SSM, the surface of the specimen was broken away during compression by liquid flow toward the surface of the specimen. The continuous decrement of the load by liquid segregation in the critical point (the specific strain value is 0.15) was not shown to be remarkable at the strain rates of 5.88 × 10^{-2} s^{-1} and 5.88 × 10^{-1} s^{-1}; however, the stress increased with the increase of strain at the strain rate of 5.88 s^{-1}.

Figure 2(c) shows the curve of true stress-true strain with various strain rates (5.88 × 10^{-2} s^{-1}, 5.88 × 10^{-1} s^{-1}, and 5.88 s^{-1}) at 565 °C corresponding to the solid fraction of 90%. The characteristics of a SSM were not detected, and it was revealed that the relationship of the stress-strain rate of the hot compression specimen was the increase of stress according to that of the strain rate.

Figure 3(a) and (b) show the relationship between stress and strain in a performed compression test to control the liquid segregation phenomenon. The compression test started at the strain rates of 5.88 × 10^{-2} s^{-1}, 5.88 × 10^{-1} s^{-1}, and 5.88 s^{-1}; then, the strain rates were increased to 5.88 × 10^{-1} s^{-1}, 5.88 s^{-1}, and 29.4 s^{-1} at the strain of 0.15, respectively. In the case of the one-step jumping strain rate in Fig. 3(a), the load was increased with the increase of the strain rate. The variation of the stress in the one-step jumping strain rate was similar to that in the two-step jumping strain rate, and the load increased continuously without the decrease by the liquid separation due to the increase of strain rate. The reason that the stress decreased

Table 1 Chemical compositions of A356, 86S, and A390 materials

Material	%	Si	Fe	Cu	Mn	Mg	Ni	Zn	Ti	Pb
A357	Min	6.5	…	…	…	0.50	…	…	…	…
	Max	7.5	0.15	0.03	0.03	0.60	0.03	0.05	0.20	0.03
86S	Min	5.0	…	2.5	0.3	…	…	…	…	…
	Max	6.5	0.15	3.5	0.03	0.04	0.03	0.05	0.20	0.3
A390	Min	16.0	…	4.0	…	0.5	…	…	…	…
	Max	17.0	0.4	5.0	0.1	0.65	0.01	0.05	0.20	0.03

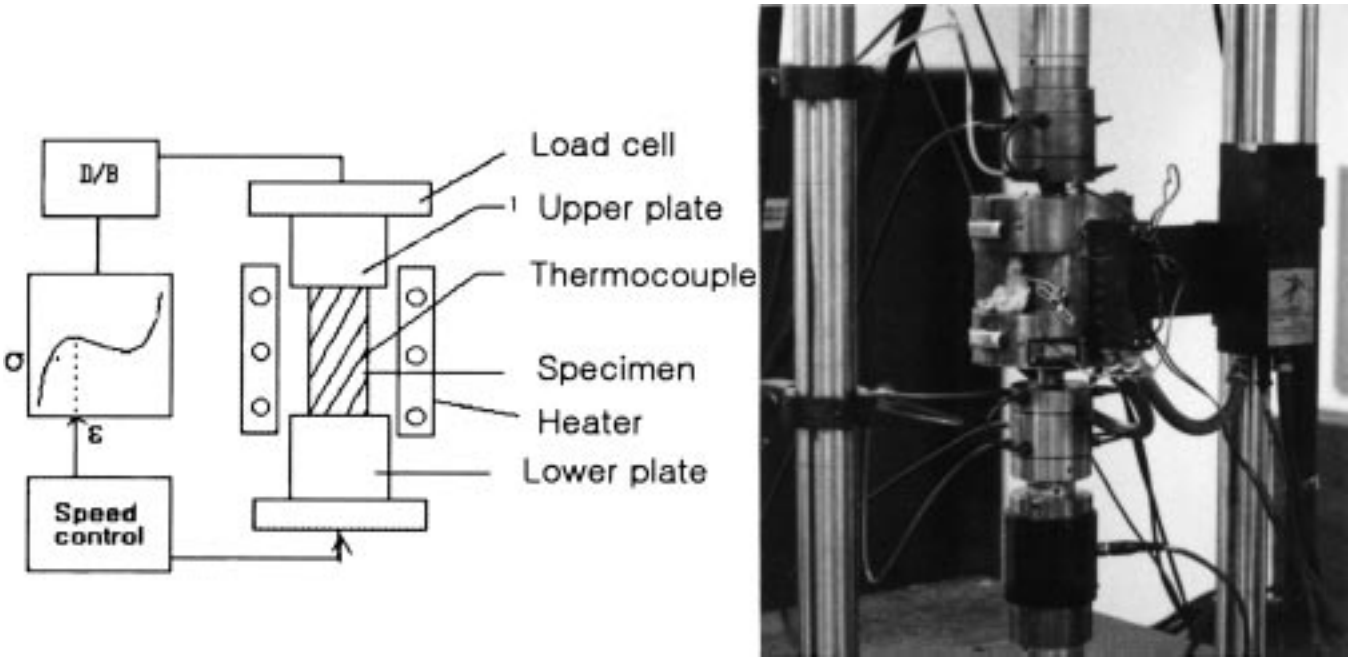

Fig. 1 Schematic diagram and testing machine for the compression test

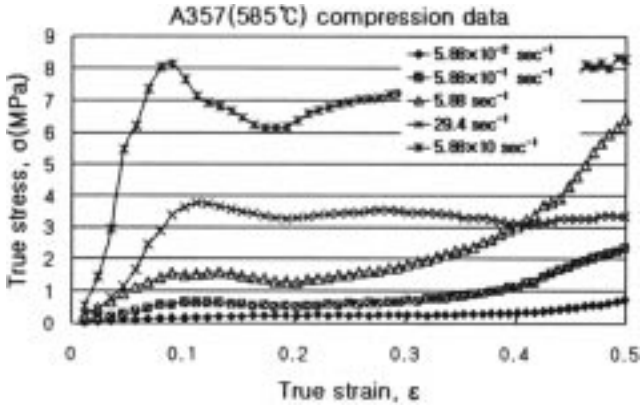

(**a**)

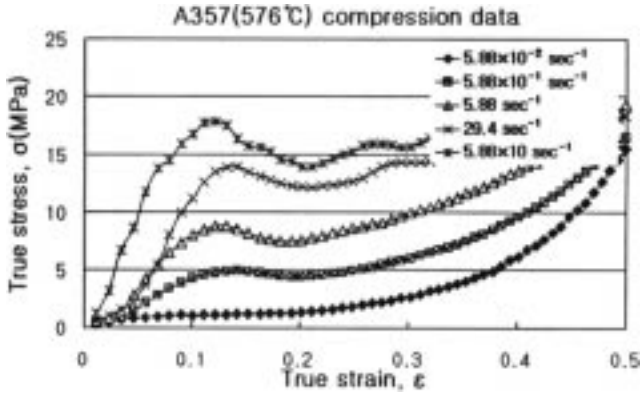

(**b**)

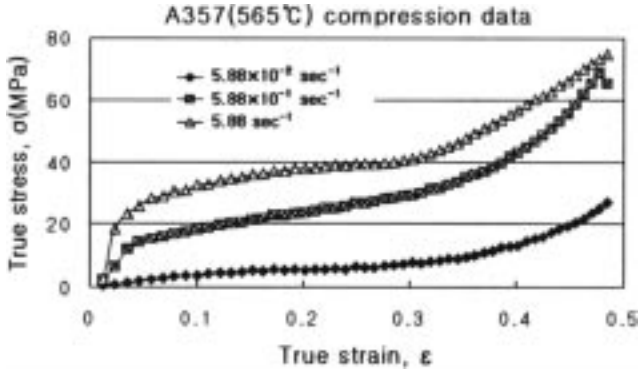

(**c**)

Fig. 2 True stress-true strain curves of A357 for various temperatures: (**a**) A357, 585 °C (f_s = 55%); (**b**) A357, 576 °C (f_s = 70%); and (**c**) A357, 65 °C (f_s = 90%)

Table 2 Temperatures of compression

	①	②	③
A357	585 °C	576 °C	565 °C
86S	577 °C	563 °C	533 °C
A390	567 °C	532 °C	…

at the point that the strain rate increased is because the discontinuity appears depending upon the sensitivity of the measuring device.

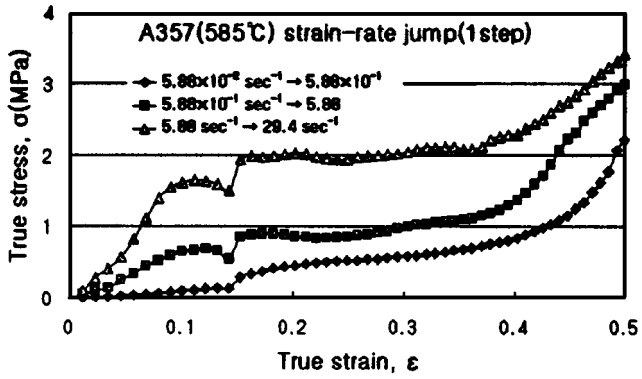

(**a**)

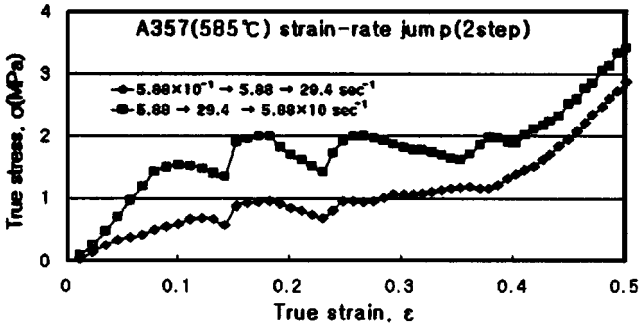

(**b**)

Fig. 3 True stress-true strain curves of A357 for various strain rates: (**a**) A357, 585 °C, one step; and (**b**) A357, 585 °C, two step

Figure 4(a) and (b) show the curve of true strain-true stress with various strain rates of the 86S alloy at 577, 563, and 533 °C, as shown in Table 2. Compared to A357, the flowability of 86S was superior to that of A357. This is because 86S contains 3% Cu, which A357 does not contain, so the wear resistance and strength are improved by age hardening.

To obtain a fine globular microstructure suitable for thixoforming, the eutectic must be melted completely at over 572 °C (complete eutectic melting temperature of the 86S alloy).[13–15] In the case of Fig. 4(b) performed at the low solid fraction with 563 °C, the decrease of the load due to the liquid separation was lower than the case of Fig. 4(a). On the other hand, the transfer of material onto the die is difficult because of the elephant foot effect at over 578 °C. From this point of view, it is better carried out at 577 °C than 563 °C.

Figure 4(c) shows the results of compression experiments performed at 533 °C corresponding to the solid fraction of 90% in 86S. In the case of the strain rate of 5.88 s^{-1}, the deformation characteristics of the SSM were not detected and it was revealed that the relation of the stress-strain rate of the hot compression specimen was the increase of stress according to that of the strain rate. However, the decrease of load was detected a little at the strain rate of 5.88×10^{-1} s^{-1}.

In the case of the solid fraction of 50%, the relationship between stress and strain is shown in Fig. 5(a). The compression tests have been performed to investigate the liquid separation of 86S material for the variation of strain rates. The compression started at the strain rates of 5.88×10^{-1} s^{-1}, 5.88×10^{-1} s^{-1}, and 5.88 s^{-1}, and then the strain rates increased to 2.353 s^{-1},

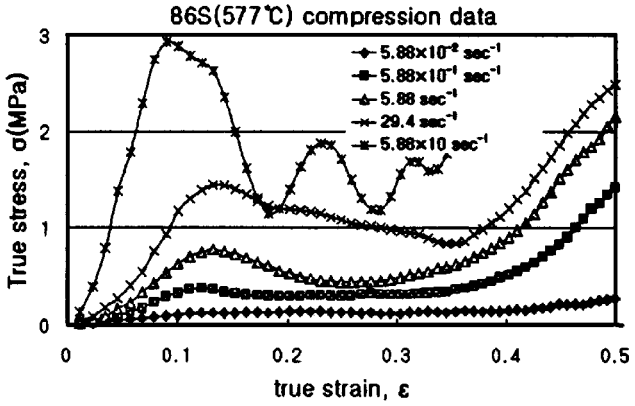

(a)

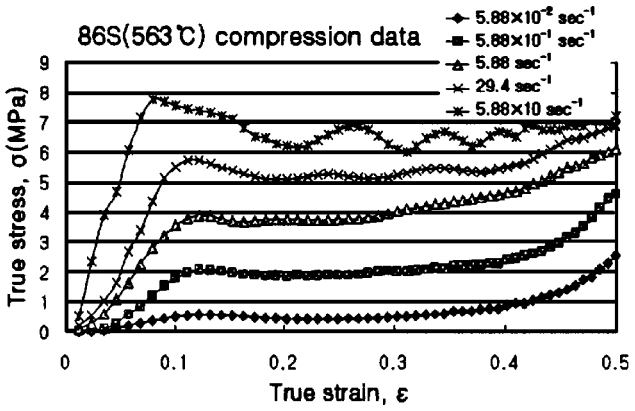

(b)

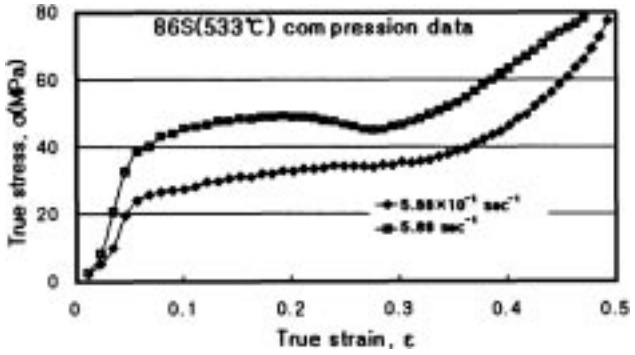

(c)

Fig. 4 True stress-true strain curves of 86S for various temperatures corresponding to the desired solid fractions of 55, 70, and 90%: (**a**) 86S, 577 °C (f_s = 55 pct); (**b**) 86S, 563 °C (f_s = 70 pct); and (**c**) 86S, 533 °C (f_s = 90%)

5.88 s^{-1}, and 29.4 s^{-1}, respectively. When the strain rate increased from 5.88 × 10^{-1} s^{-1} to 5.88 s^{-1}, the continuous increment of stress was observed. On the other hand, in the case in which the strain rate increased from 5.88 × 10^{-1} s^{-1} to 2.353 s^{-1}, this phenomenon was not detected.

As shown in Fig. 5(b), the continuous increment of load was detected in the two-step strain rate jumping process: 5.88 × 10^{-1} s^{-1} → 5.88 s^{-1} → 29.4 s^{-1} and 5.88 s^{-1} → 29.4 s^{-1} → 5.88 × 10 s^{-1}.

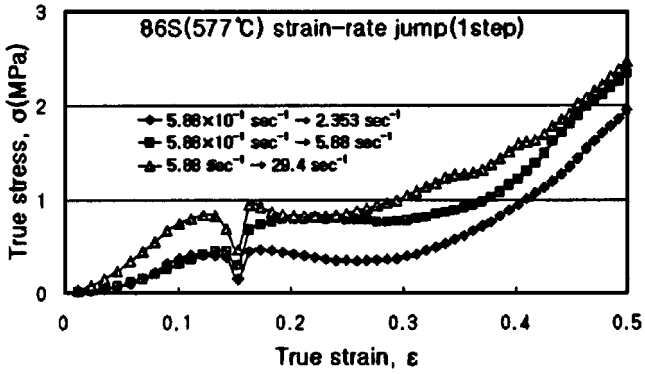

(a)

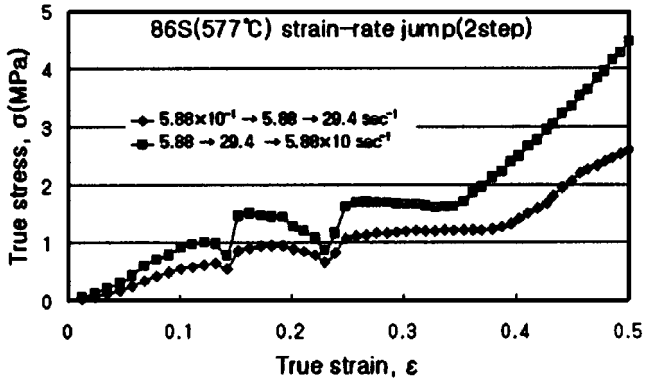

(b)

Fig. 5 True stress-true strain curves of 86S according to the increase of strain rate at each strain: (**a**) 86S, 577 °C, one-step jumping strain rate; and (**b**) 86S, 577 °C, two-step jumping strain rate

Figure 6(a) and (b) show the results of A390 material performed at the temperatures of 576 and 532 °C corresponding to the solid fractions of 55 and 70%, respectively. A390 contains 17% Si and 4% Cu, so the flowability and wear resistance of hypereutectic A390 with more Si and Cu are better than these of A357 and 86S. Therefore, we can see that, with the increasing widespread use of semisolid forming components, the development of a tailored alloy for a specific application has to be chosen. Semisolid forming the hypereutectic A390 is also a major opportunity.[13–15]

Figures 7(a) and (b) show the curve of true strain-true stress with the multistage variation of the strain rates of A390 alloy. The stress increased continuously according to the increase of strain when the strain rate was changed to one-step (5.88 × 10^{-2} s^{-1} → 5.88 × 10^{-1} s^{-1}, 5.88 × 10^{-1} s^{-1} → 2.353 s^{-1}, 2.353 s^{-1} → 7.058 s^{-1}, and 7.058 s^{-1} → 29.4 s^{-1}) and two-step (5.88 × 10^{-2} s^{-1} → 5.88 × 10^{-1} s^{-1} → 5.88 s^{-1} and 5.88 × 10^{-1} s^{-1} → 5.88 s^{-1} → 29.4 s^{-1}) at 567 °C, respectively. As mentioned above, the amount of the increased strain rate would be used for the semisolid forming process to control the liquid segregation.

2.3 Flow Stress Equation

The important factor in the semisolid forming analysis with die design is the relationship formulation between the strain

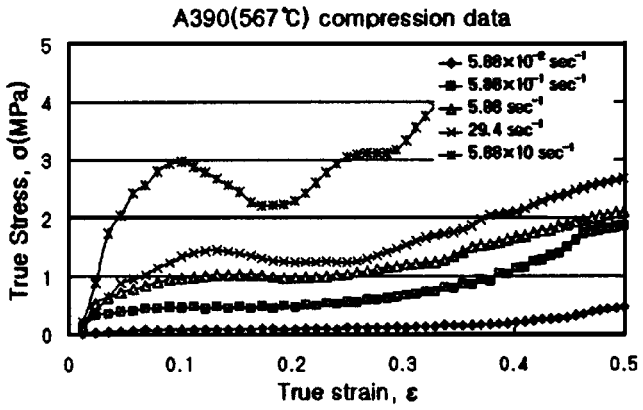

(**a**)

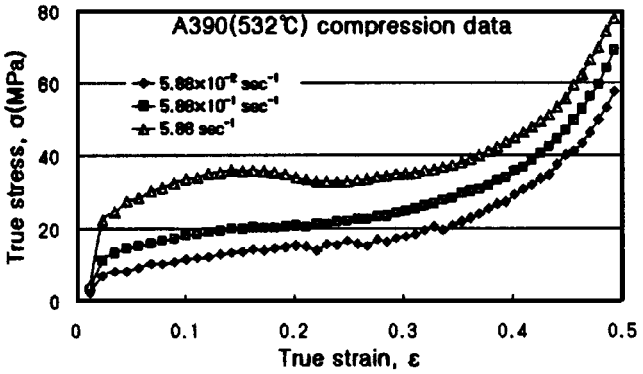

(**b**)

Fig. 6 True stress-true strain curves of A390 for various solid fractions and strain rates: (**a**) A390, 567 °C (f_s = 55 pct); and (**b**) A390, 532 °C (f_s = 70 pct)

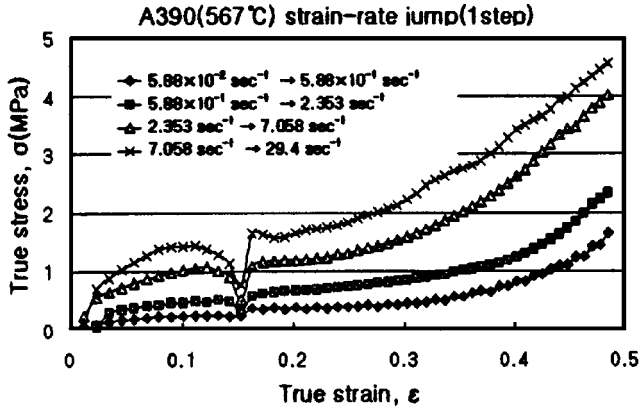

(**a**)

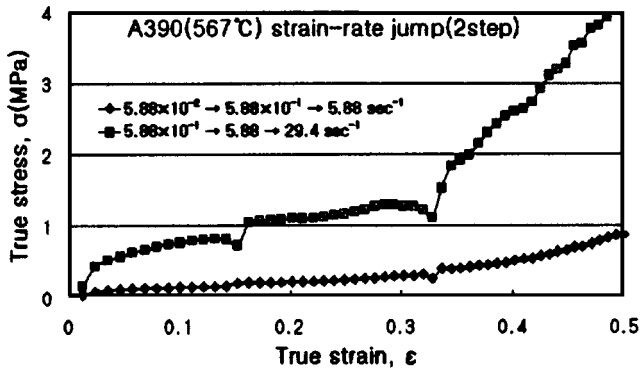

(**b**)

Fig. 7 True stress-true strain curves of A390 according to the increase of strain rate at each strain: (**a**) A390, 567 °C (f_s = 55 pct), one-step; and (**b**) A390, 567 °C (f_s = 55 pct), two-step

and the stress considering the liquid segregation and the deformation of the solid particles with a globular microstructure. By introducing the separation coefficient S, thus, the flow stress equation is suggested by correcting the relationship formulation between the stress and the strain and is represented according to the interval of the critical strain.[12,15]

$$S = S + (1 - S_0)\frac{\bar{\varepsilon}}{\varepsilon_{cr}} \qquad \text{(Eq 1)}$$

$$\varepsilon < \bar{\varepsilon}_{cr}, \varepsilon > \bar{\varepsilon}_{cr1} \qquad \text{(Eq 2)}$$

$$\bar{\sigma} = K \exp(S)\dot{\varepsilon}^m \exp\left(\frac{Q}{RT}\right)[1 - \beta f_L]^{2/3}$$

$$\bar{\varepsilon}_{cr} < \varepsilon < \bar{\varepsilon}_{cr1} \qquad \text{(Eq 3)}$$

$$\bar{\sigma} = K \exp(1 - S)\dot{\varepsilon}^m \exp\left(\frac{Q}{RT}\right)[1 - \beta f_L]^{2/3}$$

where

$\bar{\varepsilon}$ = effective stress,
$\bar{\varepsilon}_{cr}$ = primary critical strain,
K,Q,R = material constants,
T = absolute temperature,
β = geometric coefficient,
f_L = liquid fraction,
$\bar{\varepsilon}_{cr}$ = secondary critical strain, and
S_0 = dimensionless coefficient considering the agglomeration state between the solid phase and the liquid region.

The values of k and m for only A356 have been reported in a separate paper.[11,12] Therefore, the compression tests were performed to obtain the values of k and m. Figure 8 shows that the relationship of the stress-strain rate represents that of algebraic coordinates using the results of the compression test. Table 3represents the values of k and m for various temperatures and materials. The suggestion of a new strain rate is required, in which the stress increases continuously according to the increase of strain rate.

2.4 Macroscopic Structures

Figure 9 to 11 show the macroscopic structures of sectioned specimens of A357, 86S, and A390 alloys for the variations of strain rates. As shown in Fig. 9(a) and (b), in the case of constant strain rates (5.88×10^{-1} s^{-1} and 5.88×10 s^{-1}), only the solid region around the contact die deformed, the liquid region and solid particles flowing to the free surface in the middle part of the material, with the outermost material being separated from the surface. However, in the case of the increase

of strain rates (5.88×10^{-2} $s^{-1} \rightarrow 5.88 \times 10^{-1}$ s^{-1} and 5.88 $\rightarrow$ 29.4 $\rightarrow$ 5.88×10 s^{-1}), the decrease of macrosegregation was detected for a homogeneous distribution of solid particles.

Figure 9(c) shows the macrophotographs of sectioned A357 specimens for various strain rates (constant strain rate: 5.88 s^{-1}; and increase of strain rate: 5.88×10^{-1} $s^{-1} \rightarrow 5.88$ s^{-1} and 5.88×10^{-2} $s^{-1} \rightarrow 5.88 \times 10^{-1}$ $s^{-1} \rightarrow 5.88$ s^{-1}).

Figure 9(d) shows the macroscopic structures of sectioned A357 specimens for various strain rates: (1) 29.4 s^{-1}, (2) 5.88 $s^{-1} \rightarrow 29.4$ s^{-1}, and (3) 5.88×10^{-1} $s^{-1} \rightarrow 5.88$ $s^{-1} \rightarrow 29.4$ s^{-1}. Macrosegregation and porosity were reduced according to the increase of strain rate.

Figure 10(a) to (c) show the macrophotographs of sectioned 86S specimens for various strain rates: (a) (1) 5.88 s^{-1} and (2) 5.88×10^{-1} $s^{-1} \rightarrow 5.88$ s^{-1}; (b) (1) 29.4 s^{-1}, (2) 5.88 $s^{-1} \rightarrow$ 29.4 s^{-1}, and (3) 5.88×10^{-1} $s^{-1} \rightarrow 5.88$ $s^{-1} \rightarrow 29.4$ s^{-1}; and (c) (1) 5.88×10 s^{-1} and (2) 5.88 $s^{-1} \rightarrow 29.4$ $s^{-1} \rightarrow 5.88 \times 10^{-1}$ s^{-1}.

Figure 11(a) and (b) show the macroscopic behavior of sectioned A390 specimens for various strain rates: (a) (1) 5.88×10^{-1} s^{-1} and (2) 5.88×10^{-2} $s^{-1} \rightarrow 5.88 \times 10^{-1}$ s^{-1}; and (b) (1) 29.4 s^{-1}, (2) 5.88 $s^{-1} \rightarrow 29.4$ s^{-1}, and (3) 5.88×10^{-1} $s^{-1} \rightarrow 5.88$ $s^{-1} \rightarrow 29.4$ s^{-1}.

In the compression of SSMs, the increase or decrease of stress depends on the increase of strain rate. However, in the hot forging and compression forming without a globular microstructure, the material can fill a cavity with the increase of stress according to the increase of strain rate. When the compression is performed at a constant velocity, the velocity factor, where the stress increases continuously by changing the strain rate, is very important in the forging process. From the preceding results, we can see that, in the forming of SSMs, the strain rate must be controlled to increase the stress according to the increase of strain rate.

Compared to the one-step jumping strain rate, in the case of the two-step jumping strain rate, the difference of porosity and macrosegregation on the surface was not found. From the preceding result, it was found that the increment of strain rate does not affect the deformation behavior after the liquid region of the surface outflows to the surface of the material, and the solid grains and liquid phase flow simultaneously so that the stress is reduced.

The flowability of hypereutectic A390 with more Si and Cu is better than that of A357 and 86S. On the other hand, in the case of 86S, even though the composition is hypoeutectic, the deformation behavior of this alloy is similar to that of hypereutectic materials (liquid segregation and strengthening mechanism) due to the compositive actions of Si and Cu.[14–17]

Table 3 Definition of the coefficients *k* and *m* (flow stress equation: $\sigma = K\dot{\varepsilon}^m$)

Alloy	A357		86S(a)		A390
Symbol	■	◆	▲	■	●
Temperature, °C	585	565	544	563	567
k	0.65	3.4	0.32	1.57	0.34
m	0.52	0.37	0.43	0.37	0.48

(a) 86S is similar to A319

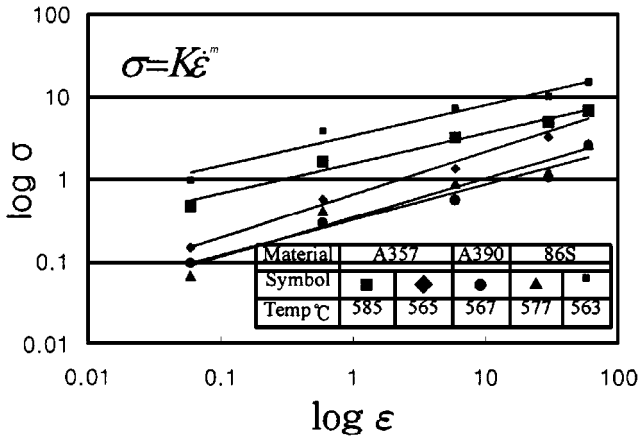

Fig. 8 Relationship between log *o* and log $\dot{\bar{\varepsilon}}$ with various materials and temperatures

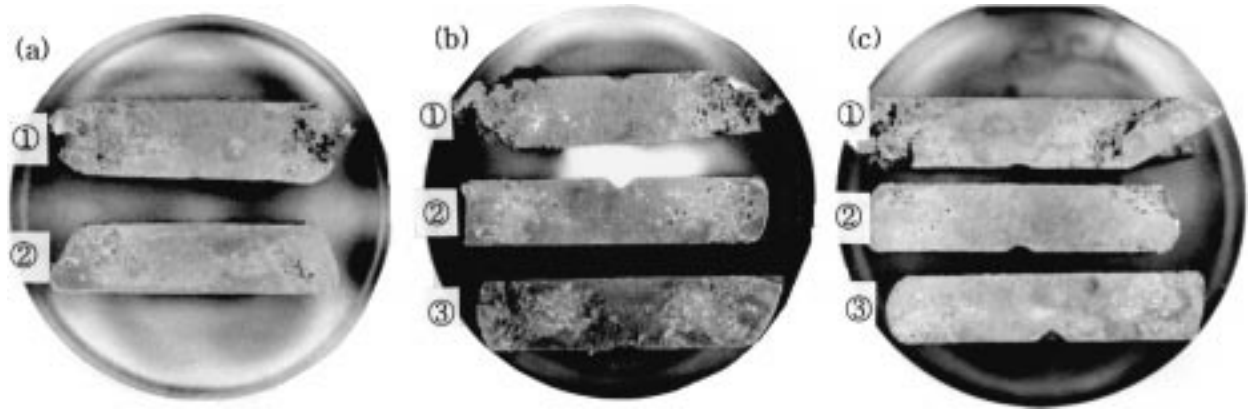

Fig. 9 Macrostructure of the sectioned specimen after the compression test with A357: (**a**) ① 5.88×10^{-1} s^{-1} and ② $5.88 \times 10^{-2} \rightarrow 5.88 \rightarrow 10^{-1}$ s^{-1}; (**b**) ① 5.88×10 s^{-1} and ② $5.88 \rightarrow 29.4 \rightarrow 5.88 \times 10$ s^{-1}; (**c**) ① 5.88 s^{-1}, $5.88 \times 10^{-1} \rightarrow 5.88$ s^{-1}, and ③ $5.88 \times 10^{-2} \rightarrow 5.88 \times 10^{-1} \rightarrow 5.88$ s^{-1}; and (**d**) ① 29.4 s^{-1}, ② $5.88 \rightarrow 29.4$ s^{-1}, and ③ $5.88 \times 10^{-1} \rightarrow 5.88 \rightarrow 29.4$ s^{-1}

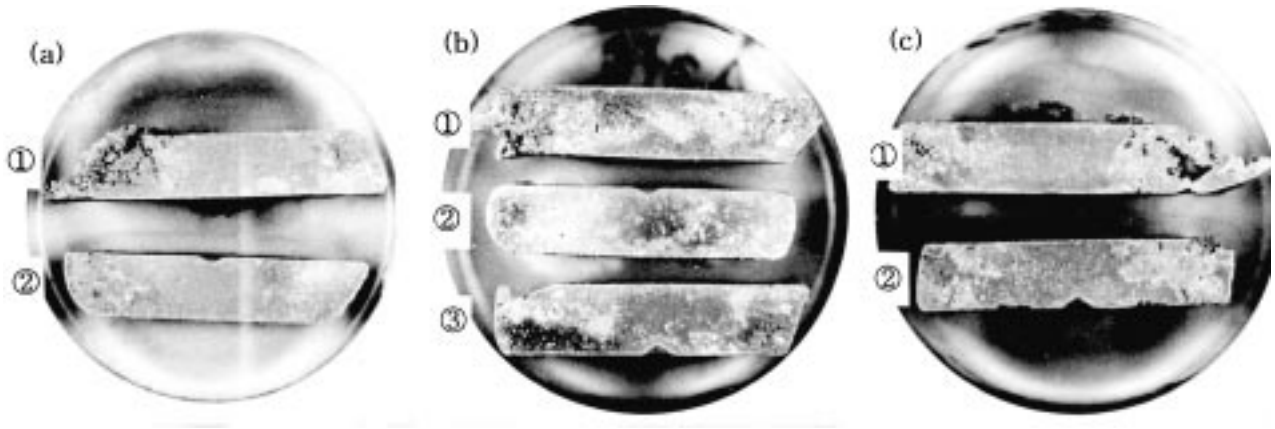

Fig. 10 Macrostructure of the sectioned specimen after compression test with 86S: (**a**) ① 5.88 s^{-1} and ② 5.88 × 10^{-1} → 5.88 s^{-1}; (**b**) ① 29.4 s^{-1}, 5.88 ② × 29.4 s^{-1}, and ③ 5.88 × 10^{-1} → 5.88 → 29.4 s^{-1}; and (**c**) ① 5.88 × 10 s^{-1} and ② 5.88 → 29.4 → 5.88 × 10^{-1} s^{-1}

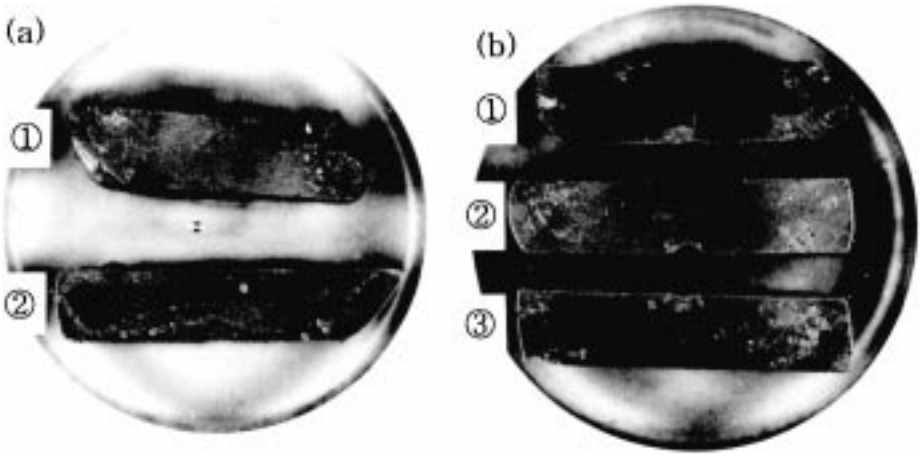

Fig. 11 Macrostructure of the sectioned specimen after compression test with A390: (**a**) ① 5.88 × 10^{-1} s^{-1} and ② 5.88 × 10^{-2} → 5.88 × 10^{-1} s^{-1}; and (**b**) ① 29.4 s^{-1}, ② 5.88 → 29.4 s^{-1}, and ③ 5.88 × 10^{-1} → 5.88 → 29.4 s^{-1}

In the case of A390, the amount of porosity and macrosegregation to the surface were reduced remarkably because of the improvement in fluidity in spite of a lower compression velocity.

2.5 Microscopic Structures

Figure 12 shows the microstructure of the compressed specimen according to the change of the strain rate after reaching the compression temperature of the desired solid fraction. The (a) center, (b) middle, and (c) surface positions in Fig. 12 are the positions to observe the deformation behavior of globularization after the compression test. As shown in Fig. 12, when the compression test was carried out at constant strain rates of 5.88 × 10^{-1} s^{-1}, 5.88 s^{-1}, 29.4 s^{-1}, and 5.88 × 10 s^{-1}, a dense microstructure was obtained at the middle position (b). However, the amount of porosities at the middle position (b) increased due to the liquid separation. In the case of surface position (c), the material deformation due to the fracture was observed. Furthermore, the occurrence of porosities was independent of the variation of the cross-sectional areas. Particularly, a uniform distribution of solid and liquid phases was obtained for a strain rate of over 5.88 s^{-1}.

Figure 13 shows the microstructure of the A357 specimen for various strain rates: (1) 5.88 × 10^{-2} s^{-1} → 5.88 × 10^{-1} s^{-1}, (2) 5.88 × 10^{-1} s^{-1} → 5.88 s^{-1}, and (3) 5.88 s^{-1} → 29.4 s^{-1}. Compared to Fig. 12, the amount of porosity was reduced and a uniform distribution of solid grains was obtained. In order to manufacture parts without defects in the compression forming with a low strain rate (5.88 × 10^{-2} s^{-1} → 5.88 × 10^{-1} s^{-1}), the decreased load must be controlled to obtain the uniform solid fraction by the continuous increase of stress with the increase of strain rate.

Figure 14 shows the microstructure of the A357 specimen for a variety of strain rates: (1) 5.88 × 10^{-2} s^{-1} → 5.88 × 10^{-1} s^{-1} → 5.88 s^{-1}, (2) 5.88 × 10^{-1} s^{-1} → 5.88 s^{-1} → 29.4 s^{-1}, and (3) 5.88 s^{-1} → 29.4 s^{-1} → 5.88 × 10 s^{-1}. The results were similar to those of Fig. 9 with a one-step jumping strain rate. The segregation phenomenon of the liquid region and the solid region appeared in the compression test of an SSM. The decrease of the load by liquid segregation in the critical point (the specific strain value is 0.15) was controlled as the increase of strain rate. In the case of the strain being over 0.15, the strain was not affected by the increase of strain rate.

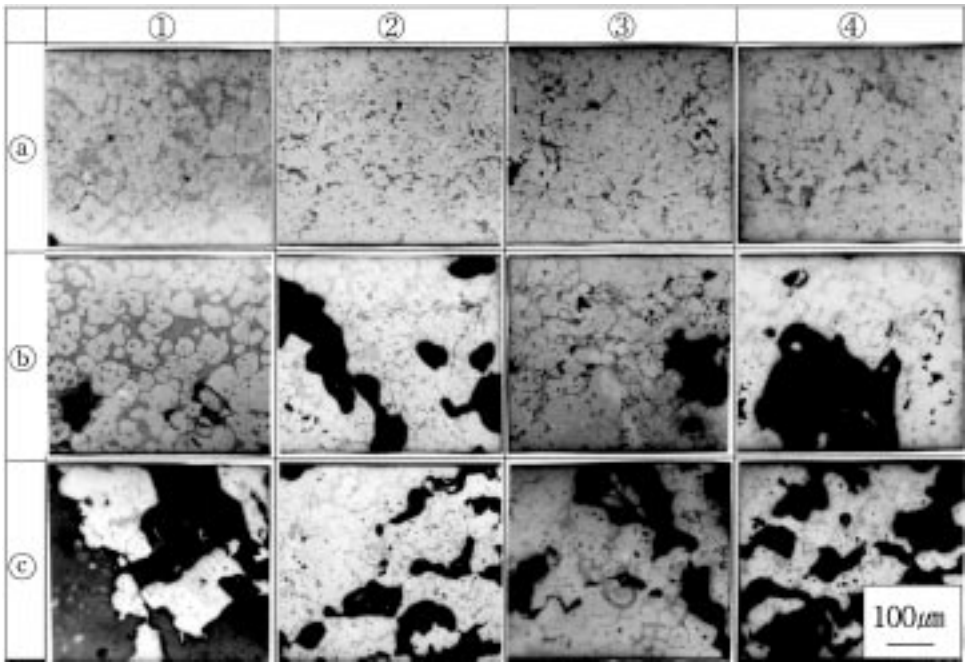

Fig. 12 Microstructure of the specimen after compression test with A357 (585 °C): ① 5.88×10^{-1} s^{-1}, ② 5.88 s^{-1}, ③ 29.4 s^{-1}, and ④ 5.88×10 s^{-1}. (**a**) Center position, (**b**) middle position, and (**c**) surface position

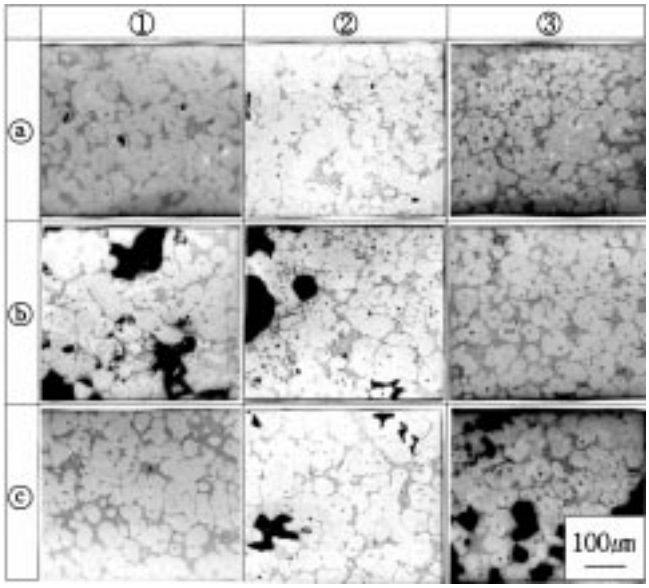

Fig. 13 Microstructure of the specimen after one-step strain-rate jump compression with A357 (585 °C): ① $5.88 \times 10^{-2} \rightarrow 5.88 \times 10^{-1}$ s^{-1}, ② $5.88 \times 10^{-1} \rightarrow 5.88$ s^{-1}, and ③ $5.88 \rightarrow 29.4$ s^{-1}. (**a**) Center position, (**b**) middle position, and (**c**) surface position

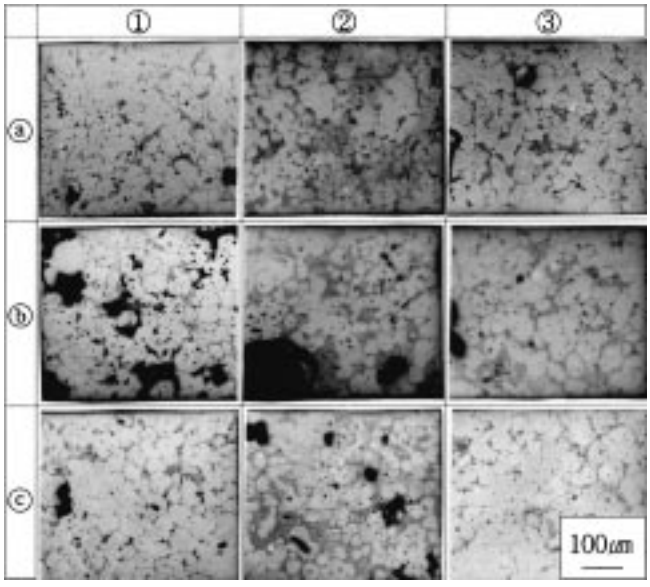

Fig. 14 Microstructure of the specimen after two-step strain-rate jump compression with A357 (585 °C): ① $5.88 \times 10^{-2} \rightarrow 5.88 \times 10^{-1} \rightarrow 5.88$ s^{-1}, ② $5.88 \times 10^{-1} \rightarrow 5.88 \rightarrow 29.4$ s^{-1}, and ③ $5.88 \rightarrow 29.4 \rightarrow 5.88 \times 10$ s^{-1}. (**a**) Center position, (**b**) middle position, and (**c**) surface position

Figure 15 shows the structural photograph of the 86S specimen at 577 °C (strain rate: 5.88 s^{-1}, 29.4 s^{-1}, 5.88×10 s^{-1}, 5.88×10^{-1} $s^{-1} \rightarrow 5.88$ s^{-1}, and 5.88 $s^{-1} \rightarrow 29.4$ s^{-1}). 86S has a low strain resistance because of the improvement in fluidity by the Cu component. Therefore, in the case of 86S, the occurring possibility of porosity is lower than that of A357 at constant compression velocities. Based on the preceding results, from the point of view of preventing the liquid segregation by the increment of strain rate, the use of 86S is more highly recommended than that of A357.

Figure 16 shows the microstructure of the compressed A390 specimen at 567 °C (strain rate: 5.88×10^{-1} s^{-1}, 29.4 s^{-1}, 5.88×10^{-2} $s^{-1} \rightarrow 5.88 \times 10^{-1}$ s^{-1}, 7.05 $s^{-1} \rightarrow 29.4$ s^{-1}, and 5.88×10^{-1} $s^{-1} \rightarrow 5.88$ $s^{-1} \rightarrow 29.4$ s^{-1}). Unlike

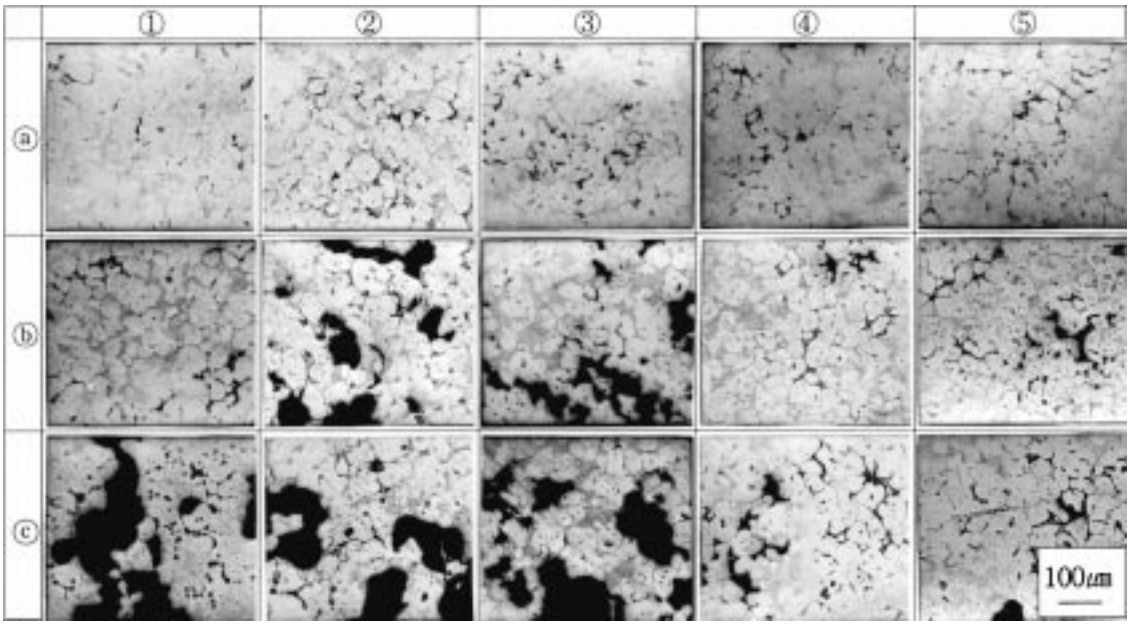

Fig. 15 Microstructure of the specimen after compression test with 86S (577 °C): ① 5.88 s^{-1}, ② 29.4 s^{-1}, ③ 5.88 × 10 s^{-1}, ④ 5.88 × 10^{-1} → 5.88 s^{-1}, and ⑤ 5.88 → 29.4 s^{-1}. (**a**) Center position, (**b**) middle position, and (**c**) surface position

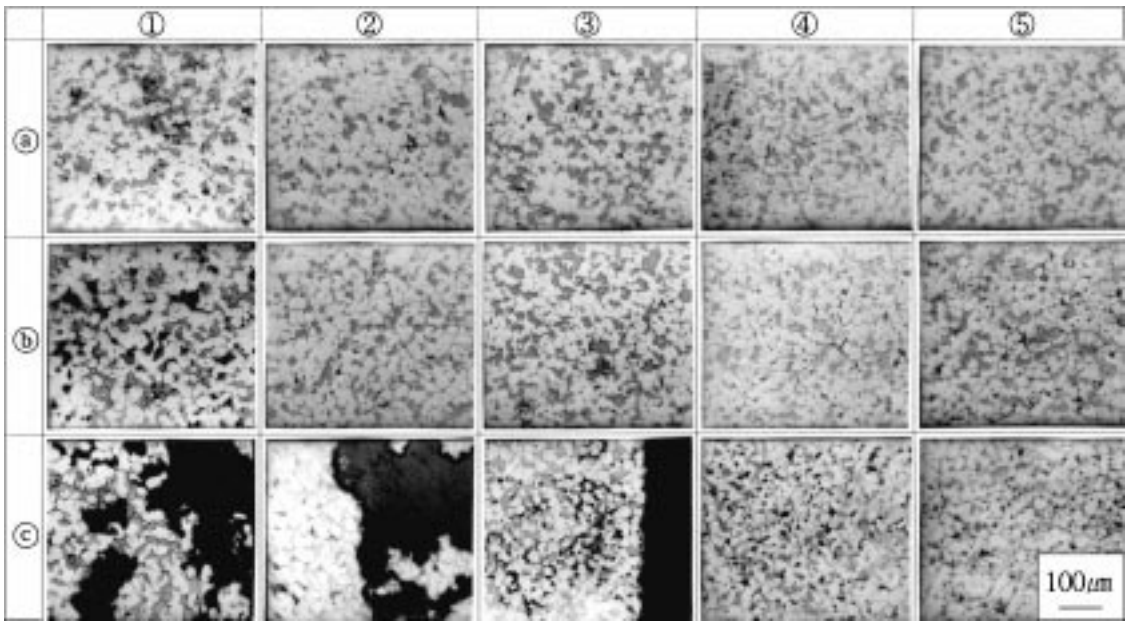

Fig. 16 Microstructure of the specimen after compression test with A390 (567 °C): ① 5.88 × 10^{-1} s^{-1}, ② 29.4 s^{-1}, ③ 5.88 × 10^{-2} → 5.88 × 10^{-1} s^{-1}, ④ 7.05 → 29.4 s^{-1}, and ⑤ 5.88 × 10^{-1} → 5.88 → 29.4 s^{-1}. (**a**) Center position, (**b**) middle position, and (**c**) surface position

A357 and 86S, in the case of the compressed A390 specimen with constant velocities, porosity was not observed at the middle position (b). The porosity by cracking on the surface of the specimen was only observed at the surface position (c).

The reason for the above is that, the greater the Si content, the more difficult it is for the solid phase to be separated from the liquid phase. The fracture on the free surface was reduced remarkably because of the increase of strain rate. Uniform microstructures without porosity were also obtained in the overall cross-sectional areas. From the preceding result, it is found that, the lower the deformation resistance in the semisolid state, the lower is the occurring possibility of porosities due to the liquid separation. Finally, it was concluded that, to improve the semisolid formability and to reduce the occurring possibility of defects, the liquid segregation should be controlled as the multistage increase of the strain rate during compression forming. The results of com-

pression tests proposed in this work would contribute to the reduction of many lead times for manufacturing and promotion of the semisolid forming process.

3. Conclusions

Based on compression tests of semisolid aluminum materials for a variety of strain rates, the conclusions can be summarized as follows.

- For the deformation characteristics of the SSM, the stress increased up to a specific strain value of 0.1. However, from the strain of $\varepsilon = 0.1$, the stress decreased remarkably when the strain rate increased.
- In the case of the one-step jumping strain rate, the load was increased with the increase of strain rate. The variation of the stress in the one-step jumping strain rate was similar to that in the two-step jumping strain rate, and the load increased continuously without the decrease by the liquid separation due to the increase of strain rate.
- In order to manufacture parts without defects in the compression forming with a low strain rate, the decreased load must be controlled to obtain the uniform solid fraction by the continuous increase of stress with the increase of strain rate.
- In the case of hypereutectic A390, the amounts of porosity and macrosegregation to the surface were reduced remarkably because of the improvement in fluidity in spite of a lower compression velocity.
- In the case of A390, the occurring possibility of defects was lower than that of A357 and 86S at constant compression velocities. Based on the preceding results, from the point of view of preventing the liquid segregation by the increment of strain rate, the use of A390 was more highly recommended than that of A357 and 86S.
- It was concluded that, to improve the semisolid formability and to reduce the occurring possibility of defects, the liquid segregation should be controlled as the multistage increase of the strain rate during compression forming.

Acknowledgments

Support for this work was provided by the Engineering Research Center for Net Shape and Die Manufacturing (ERC/NSDM), which is an excellent center appointed by the Korea Science and Engineering Foundation (KOSEF).

References

1. H.E. Pitts and H.V. Atkinson: *Proc. 5th Int. Conf. on Semi-Solid Processing of Alloys and Composites*, Golden, CO, June 1998, A.K. Bhasin, J.J. Moore, K.P. Young, and S. Midson, eds., Colorado School of Mines, Golden, CO, 1998, pp. 97-104.
2. D.H. Kirkwood: *Int. Mater. Rev.*, 1994, vol. 39 (5), pp. 173-89.
3. H.K. Jung, C.G. Kang, and Y.H. Moon: *J. Mater. Eng. Performance*, 2000, vol. 9 (1), pp. 12-23.
4. H.K. Jung and C.G. Kang: *Key Eng. Mater.*, 2000, vol. 177-180, pp. 571-76.
5. H.K. Jung and C.G. Kang: *Proc. 8th Int. Symp. on Plasticity and Its Current Applications (PLASTICITY2000)*, A.S. Khan, ed., 2000, pp. 240-42.
6. M. Suery and M.C. Flemings: *Metall. Trans. A*, 1982, vol. 13A, pp. 1809-19.
7. C. Yoshida, M. Moritaka, S. Shinya, K. Takebayashi, and A. Nanba: *Proc. 2nd Int. Conf. on Semi-Solid Processing of Alloys and Composites*, M.C. Flemings and S.B. Brown, eds., Massachusetts Institute of Tech., Cambridge, MA, June 10–12, 1992, pp. 95-102.
8. J.S. Gunasekera: *Proc. 2nd Int. Conf. on Semi-Solid Processing of Alloys and Composites*, M.C. Flemings and S.B. Brown, eds., Massachusetts Institute of Tech., Cambridge, MA, June 10–12, 1992, pp. 211-22.
9. D.A. Pinsky, P.O. Charreyron, and M.C. Flemings: *Metall. Trans. B*, 1984, vol. 15B, pp. 173-81.
10. M. Kiuchi, S. Sugiyama, and Y. Hisata: *Jpn. Diecasting Congr. Trans.*, 1998, pp. 151-56.
11. C.G. Kang, J.S. Choi, and K.H. Kim: *J. Mater. Processing Techol.*, 1999, vol. 88, pp. 159-68.
12. C.G. Kang and H.K. Jung: *Int. J. Mech. Sci.*, 1999, vol. 14 (12), pp. 1423-45.
13. M. Garat, S. Blais, C. Pluchon, and W.R. Loue: *Proc. 5th Int. Conf. on Semi-Solid Processing of Alloys and Composites*, A.K. Bhasin, J.J. Moore, K.P. Young, and S. Midson, eds., Golden, Colorado, June 23–25, 1998, pp. 17-31.
14. H.K. Jung and C.G. Kang: *Metall. Mater. Trans. A*, 1999, Nov., vol. 30A, pp. 2967-77.
15. C.G. Kang and H.K. Jung: *Metall. Mater. Trans. B*, 2001, vol. 32B, February 2001, pp. 129-36.
16. H.K. Jung and C.G. Kang: *Key Eng. Mater.*, 2000, vol. 177-180, pp. 565-70.
17. H.K. Jung, P.K. Seo, and C.G. Kang: *J. Mater. Processing Technol.*, 2001, 5108 (2001) 1-6.